Expression and regulatory network of long noncoding RNA in rats after spinal cord hemisection injury

From the Contents

Wei Liu[1, #], Jin-Cheng Tao[2, #], Sheng-Ze Zhu[2], Chao-Lun Dai[2], Ya-Xian Wang[1], Bin Yu[1], Chun Yao[1, *], Yu-Yu Sun[3, *]

Graphical Abstract *Expression and regulatory network of long noncoding RNA after spinal cord injury*
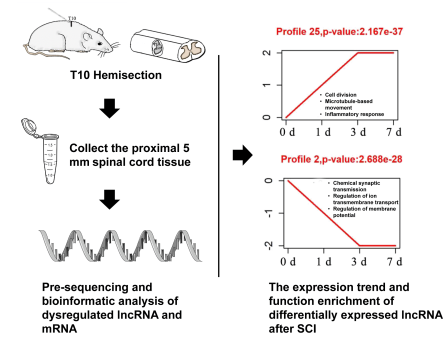
Abstract

Long noncoding RNAs (lncRNAs) participate in a variety of biological processes and diseases. However, the expression and function of lncRNAs after spinal cord injury has not been extensively analyzed. In this study of right side hemisection of the spinal cord at T10, we detected the expression of lncRNAs in the proximal tissue of T10 lamina at different time points and found 445 lncRNAs and 6522 mRNA were differentially expressed. We divided the differentially expressed lncRNAs into 26 expression trends and analyzed Profile 25 and Profile 2, the two expression trends with the most significant difference. Our results showed that the expression of 68 lncRNAs in Profile 25 rose first and remained high 3 days post-injury. There were 387 mRNAs co-expressed with the 68 lncRNAs in Profile 25. The co-expression network showed that the co-expressed genes were mainly enriched in cell division, inflammatory response, FcγR-mediated cell phagocytosis signaling pathway, cell cycle and apoptosis. The expression of 56 lncRNAs in Profile2 first declined and remained low after 3 days post-injury. There were 387 mRNAs co-expressed with the 56 lncRNAs in Profile 2. The co-expression network showed that the co-expressed genes were mainly enriched in the chemical synaptic transmission process and in the signaling pathway of neuroactive ligand-receptor interaction. The results provided the expression and regulatory network of the main lncRNAs after spinal cord injury and clarified their co-expressed gene enriched biological processes and signaling pathways. These findings provide a new direction for the clinical treatment of spinal cord injury.

Key Words: bioinformatic analysis; biological process; gene ontology analysis; inflammatory response; Kyoto encyclopedia of genes and genomes analysis; long noncoding RNAs; regulatory network; RNA sequencing; spinal cord injury; synaptic transmission

Introduction

Injury to the central nervous system includes brain injury and spinal cord injury (SCI), which often results in losing part or all of the sensory and motor functions distal to the injury site. SCI causes great pain to patients and the time and money spent on medical care bring a heavy burden to the family of patients (Lin, 2019). In the past, it was generally thought that the central nervous system of adult mammals could not regenerate. The main reasons are that the neurons in the central nervous system have lose the ability to regeneration at maturity (Kwon et al., 2016) and that the microenvironment of the central nervous system after injury is not conducive to nerve regeneration (Tedeschi and Bradke, 2017; Yang et al., 2021; Bai et al., 2021).

SCI is identified as the injury caused by direct or indirect external factors. There are various clinical and pathological changes after SCI, both motor and sensory, including sphincter dysfunction and abnormal muscle tension. After the physical injury, a series of physiological and pathological responses follow: (i) Local ischemia, edema and other severe inflammatory responses resulting from vascular rupture (Mortazavi et al., 2015), (ii) Neuronal degeneration, apoptosis and autophagy, (iii) Nerve regeneration controlled by astrocytes that promote it in the early stage and inhibit it in the late stage and (iv) Inflammation aggravated by macrophage activation (Fitch and Silver, 2008). The combined effect of the above physiological and pathological responses leads to an unfavorable microenvironment for nerve regeneration.

In the human genome, about 50% of DNA can be transcribed into RNA. However, mRNA accounts for only 1.2% of the transcribed RNA, and the remaining RNA, termed noncoding RNA, cannot be translated into proteins (Jarroux et al., 2017). Among them, a class of noncoding RNAs with a length of more than 200 nucleotides (nt) are termed long noncoding RNAs (lncRNAs) (Wilusz et al., 2009; Zhang et al., 2019). A large number of studies have explored mRNA levels during the functional repair after SCI, in particular the phosphatase and tensin homolog deleted on chromosome ten (PTEN), which defies the traditional view that the central nervous system cannot be repaired (Ohtake et al., 2014). However, there have been few studies on the expression and role of lncRNAs after SCI. The co-expression of lncRNAs with mRNAs suggests the importance of understanding the role of lncRNAs when developing new therapies to regulate the physiological and pathological responses after injury and to improve rehabilitation.

This study selected the hemisection SCI model with its high repeatability (Kozuka et al., 2016). In the 7 days following injury, we compared the changes of lncRNAs and mRNAs in the sham group with those of the SCI group to identify differentially expressed lncRNAs and mRNAs. The results would clarify the enriched biological processes involving lncRNA and their co-expressed genes after the hemisection SCI.

[1]Key Laboratory of Neuroregeneration of Jiangsu and Ministry of Education, Co-innovation Center of Neuroregeneration, Nantong University, Nantong, Jiangsu Province, China; [2]Medical College, Nantong University, Nantong, Jiangsu Province, China; [3]Department of Orthopedics, Nantong Third People's Hospital, Nantong University, Nantong, Jiangsu Province, China
*Correspondence to: Chun Yao, PhD, yaochun@ntu.edu.cn; Yu-Yu Sun, MD, sunyuyunt@126.com.
https://orcid.org/0000-0002-9742-8139 (Wei Liu)
#Both authors contributed equally to this work.

Materials and Methods

Animal surgery

The animal experiments were ethically approved by the Administration Committee of Experimental Animals, Jiangsu Province, China (approval No. 20180304-008) on March 4, 2018. For the convenience of animal care, female Sprague-Dawley rats (aged 2 months old; weight 200–220 g), approved by the Administration Committee of Experimental Animals, Jiangsu Province, China (license Nos. SCXK (Su) 2019-0001 and SYXK (Su) 2017-0046), were used in this study. The rats were raised in the specific-pathogen-free conditions, with only five rats in each cage (temperature 22°C, humidity 50–65%, 12/12-hour light/dark and had free access to food and water). All animal experiments were conducted according to the nursing guidelines of Experimental Animal Center of Nantong University and were designed and reported according to the Animal Research: Reporting of *In Vivo* Experiments (ARRIVE) guidelines (Percie du Sert et al., 2020).

In this study, rats were allocated to the two groups using the random principle. In the sham group (*n* = 72) T10 was only exposed. In the SCI group (*n* = 72), the spinal cord was exposed after resection of T10 lamina with the right hemisection. During the operation, rats were given an intraperitoneal injection of compound anesthetics (85 mg/kg chloral hydrates, 42 mg/kg magnesium sulphates and 17 mg/kg pentobarbital sodium: MilliporeSigma, Burlington, MA, USA and Merck KGaA, Darmstadt, Germany). When the rats were completely anesthetized, they were placed on a 37°C thermostatic electric blanket. Christensen's surgical method was used (Christensen et al., 1996) where the skin, fascia, and muscle were longitudinally cut at T9–T10, and the T10 lamina was removed to expose the spinal cord to perform a right hemisection using an ophthalmic iris knife (Beaver-Visitec International, Waltham, MA, USA; Wu et al., 2019). After the operation, the muscles, fascia and skin were sutured with absorbable sutures. When the rats were fully awake, they were moved to a clean and dry cage and provided with sufficient water and organic feed.

RNA-sequencing and bioinformatic analysis

The rats selected at each time point after injury, days 0 (immediately after the injury), 1, 3, 7, were given an intraperitoneal injection of compound anesthetics during the operation to collect 5 mm of spinal cord tissue, proximal to the injury. When the operation was complete, each rat was sacrificed by an injection of excess compound anesthetic. To achieve three repeated samples at each time point, a sample was taken from each of six rats to reduce the impact of individual differences. The total RNA from spinal cord tissue was extracted by the mirVana miRNA isolation kit (Ambion, Austin, TX, USA) and sequenced by Shanghai OE Biotechnology Co., Ltd. (Shanghai, China). The RNA library was sequenced on the Illumina HiSeq X10 platform (Illumina, Santiago, CA, USA) and produced 150-bp pair-end reads. First, the NGS QC Toolkit (http://www.nipgr.res.in/ngsqctoolkit.html) was used to process the raw data (the original reads) of FASTO format, and RPM (reads, mapped by splicing, per million) was taken as the expression of lncRNA and mRNA. Differential expression analysis was conducted using DESeq R package (www.Bioconductor.org) (Anders and Huber, 2010). LncRNAs with fold change > 2 and *P*-value ≤ 0.05 were considered as differentially expressed. The differentially expressed lncRNAs and mRNAs that overlapped between the sham and the SCI groups were removed, and the remainder was identified as differentially expressed lncRNAs and mRNAs after SCI. The *P*-value was then calculated for each lncRNA and mRNA (negative binomial distribution test), and the *P*-value was corrected for multiple hypothesis tests using the false discovery rate error control method to obtain a *Q*-value. Unsupervised hierarchical clustering was performed on differently expressed lncRNA and mRNA, then the expression patterns of differentially expressed genes in different samples were displayed in the form of heat maps. The STEM software (http://www.sb.cs.cmu.edu/stem/) was used to describe the expression trend diagram for time series analysis of different sample materials.

Gene ontology (GO) (The Gene Ontology Consortium, 2019) and KEGG (Kyoto Encyclopedia of Genes and Genomes) analyses were conducted, according to the previous method (Mi et al., 2017). The GO were obtained from the mapped translated protein sequences and homology searches against Swissprot using BLASTX in DIAMOND v0.9.30 (University of Tübingen, Tübingen, Germany) with an E-value cut-off of 1 × e−5 to retrieve the identifier (ID) mapping. The KEGG annotation was obtained by submitting the coding sequences of mapped genes onto the KASS-KEGG Automatic Annotation Server (Kyoto University, Kyoto, Japan). Enrichment analysis was performed via a hypergeometric test and statistical significance was considered at *P* ≤ 0.05 (Shanghai OE Biotechnology Co., Ltd.).

Real-time polymerase chain reaction

We collected total RNA from the proximal 5 mm spinal cord tissues after SCI with TRIzol reagent (Gibco, Grand Island, NY, USA). HiScript III RT SuperMix 100 for qPCR (+gDNA wiper) (Vazyme, Nanjing, China) was used to reverse transcript RNA into complementary DNA. Real-time polymerase chain reaction was performed with ChamQ SYBR qPCR Master Mix (Vazyme) on a StepOne Real-time PCR System (Applied Biosystems, Foster City, CA, USA). Primer sequences were listed in **Additional Table 1**. The results were calculated by $2^{-\Delta CT}$.

Statistical analysis

No statistical methods were used to predetermine sample sizes; however, our sample sizes were similar to those reported in a previous publication (Wu et al., 2019). There was no loss of experimental animals. All evaluators were blinded to the animal groups. Data processing and analysis were performed using GraphPad 8 (GraphPad Software, Inc., La Jolla, CA, USA, www. graphpad.com) and SPSS 20.0 (IBM, Armonk, NY, USA) statistical analysis software. We used Student's *t*-test for RT-PCR to analyze the difference between groups with double tail test. One-way analysis of variance was performed for the sham and the SCI groups respectively to exclude the differentially expressed lncRNAs and mRNAs which overlapped both the sham and SCI groups. The mean and standard error (SEM) were then calculated. *P* < 0.05 was considered statistically significant.

Results

Differentially expressed lncRNAs in proximal spinal cord after SCI

We used a rat T10 hemisection injury model to detect the lncRNA changes after SCI. RNA-sequencing analysis was carried out on the proximal hemisection spinal cord tissue at different time points after SCI. Depending on the standard of *Q*-value less than 0.01, there were 445 differentially expressed lncRNAs between the sham and SCI groups (**Figure 1A** and **Additional Table 2**) and 6522 differentially expressed mRNAs (**Figure 1B** and **Additional Table 3**) after spinal cord hemisection injury. In the heat map of lncRNAs and mRNAs, we found that the expression trend of lncRNAs and mRNAs at day 0 were similar to that of day 1, while those at days 3 and 7 were similar.
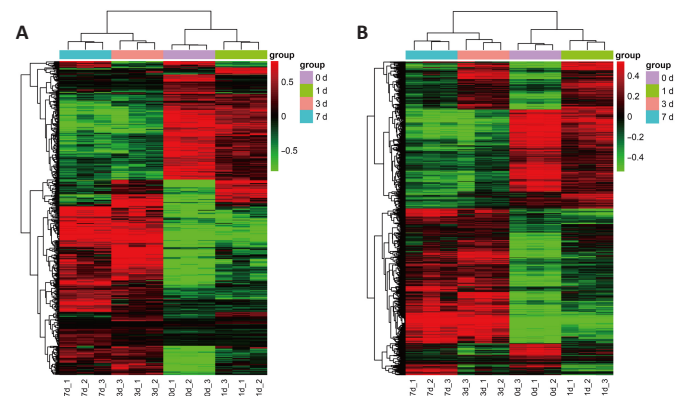

Figure 1 │ Bioinformatic analysis of dysregulated lncRNA and mRNA after spinal cord injury.
(A) Heatmap of dysregulated lncRNAs at 0, 1, 3, and 7 days after spinal cord injury. The *X*-axis is the sample name. The *Y*-axis is the name of lncRNAs, and their detailed names are in the Additional Table 2. (B) Heatmap of dysregulated mRNAs at 0, 1, 3, and 7 days after spinal cord injury. The *X*-axis is the sample name. The *Y*-axis is the name of lncRNAs, and their detailed names are in the Additional Table 3. The expression trends of lncRNAs and mRNAs on day 0 were similar to that on day 1, whereas those on day 3 were similar to day 7. Red indicates up-regulated RNAs while green indicates down-regulated RNAs. 0 d_1: The sample 1 of 0 day; 0 d_2: the sample 2 of 0 day; 0 d_3: the sample 3 of 0 day; 1 d_1: the sample 1 of 1 day; 1 d_2: the sample 2 of 1 day; 1 d_3: the sample 3 of 1 day; 3 d_1: the sample 1 of 3 days; 3 d_2: the sample 2 of 3 days; 3 d_3: the sample 3 of 3 days; 7 d_1: the sample 1 of 7 days; 7 d_2: the sample 2 of 7 days; 7 d_3: the sample 3 of 7 days; LncRNA: long noncoding RNA; mRNA: messenger RNA.

As shown in **Figure 2**, we divided the differentially expressed lncRNAs into 26 expression trends. Among them, eight trend profiles had significant *P*-value, shown in red. We then picked two tendencies with the most significant difference, Profile 25 and Profile 2, for validation. Interestingly, expressions of lncRNAs in Profile 25 rose at first and then plateaued while expressions of lncRNAs in Profile 2 declined over the first three days and then remained constant.

Functional analysis of differentially expressed lncRNAs in Profile 25

After SCI the expressions of the lncRNAs in Profile 25 rose first and then remained high after 3 days. There were 68 lncRNAs in Profile 25 (**Figure 3A**). We then randomly selected NONRATT001559.2, NONRATT005821.2, NONRATT027850.2 and NONRATT020851.2 for RT-PCR validation. The RT-PCR results of the selected lncRNAs were very consistent with the sequencing data (**Figure 3B**).

There were 387 mRNAs co-expressed with the 68 lncRNAs in Profile 25. A co-expression network was constructed for the differentially expressed lncRNAs and co-expressed mRNAs in Profile 25 (**Figure 3C**) to show the interactions between lncRNAs and mRNAs (**Additional Table 4**).

GO term enrichments were performed for the co-expressed mRNAs in Profile 25. The top 20 GO terms are shown, which suggest that the co-expressed genes were mainly enriched in processes of cell division and inflammatory response (**Figure 3D** and **Additional Table 5**). KEGG signaling pathway enrichment analysis was also conducted for the co-expressed mRNAs in Profile 25. The top 20 pathways are shown, which suggest that the co-expressed genes were mainly enriched in the FcγR-mediated cell phagocytosis signaling pathway, cell cycle and apoptosis (**Figure 3E** and **Additional Table 6**). The functional analysis of co-expressed genes in Profile 25 indicated that the lncRNAs in this profile were involved in cell cycle, apoptosis and inflammation.
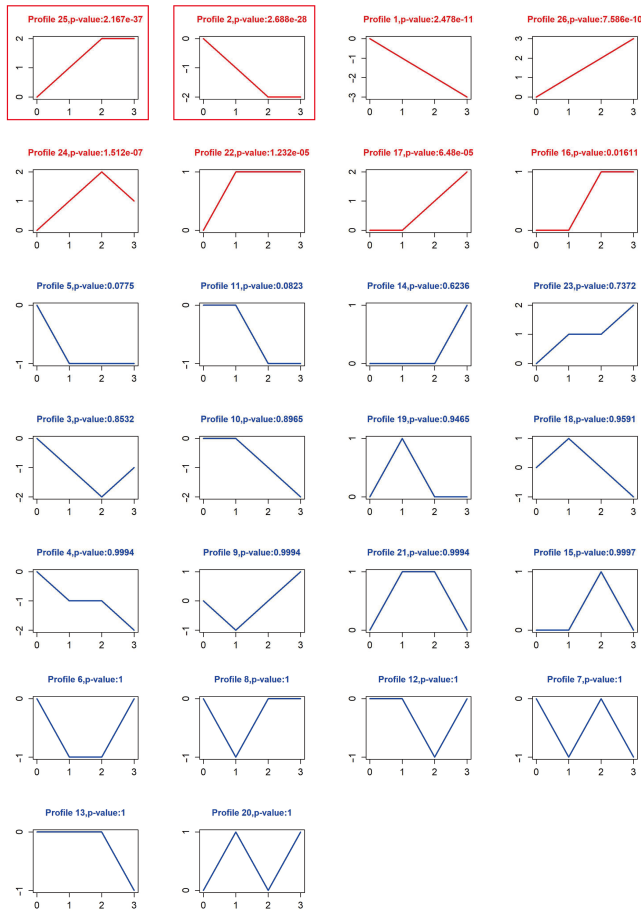
Figure 2 | Bioinformatic analysis of the expression trend of differentially expressed lncRNA after SCI.
Trends with significant difference (*P* < 0.05) were marked in red. 0 to 3 indicate days 0, 1, 3 and 7, respectively. The vertical axis indicates the overall trend of all lncRNAs in a module. LncRNA: Long noncoding RNA; SCI: spinal cord injury.

Functional analysis of differential expression lncRNAs in Profile 2

The expressions of lncRNAs in Profile 2 declined first and then remained low after 3 days post-injury. There were 56 lncRNAs in Profile 2 (**Figure 4A**). We then randomly selected NONRATT002333.2, NONRATT009996.2, NONRATT026122.2 and TCONS_00083425_novel for RT-PCR validation. The RT-PCR results of selected lncRNAs were very consistent with the sequencing data (**Figure 4B**).

There were 387 mRNAs co-expressed with the 56 lncRNAs in Profile 2. A co-expression network was constructed for the differentially expressed lncRNA and co-expressed mRNA in Profile 2 (**Figure 4C**) to show the interactions between lncRNAs and mRNAs (**Additional Table 7**).

GO term enrichments were performed for the co-expressed mRNAs in Profile 2. The top 20 GO terms are shown, which suggested that the co-expressed genes were mainly enriched in the chemical synaptic transmission process (**Figure 4D** and **Additional Table 8**). KEGG signaling pathway enrichment analysis was conducted for the co-expressed mRNAs in Profile 2. The top 20 pathways are shown, which suggest that the co-expressed genes were mainly enriched in the signaling pathway of neuroactive ligand-receptor interaction (**Figure 4E** and **Additional Table 9**).

Discussion

SCI continues to be a difficult global clinical problem. Rehabilitation and treatments after injury often bring a heavy economic burden on patients and their families. In recent years, many researchers have devoted much effort to improve regeneration and rehabilitation after SCI, but with limited effect. In this study, we analyzed the whole transcriptome of the injured spinal cord and identified dysregulated lncRNAs after SCI.

SCI is divided into primary injury and secondary injury. Primary injury is often caused by sudden spinal trauma. Subsequently, primary injury induces secondary injury, causing further chemical and mechanical injury to spinal cord tissue (Orr and Gensel, 2018). Secondary injury can be divided into three stages: acute (0–48 hours), sub-acute (first 2 weeks) and chronic injury (from days to years) (Anjum et al., 2020; Zhu et al., 2021). The acute injury stage mainly includes vascular damage, ionic imbalance, excitotoxicity, free radical production, increased calcium influx, lipid peroxidation, inflammation, oedema and necrosis (Phang et al., 2015; Alizadeh et al., 2019). The sub-acute
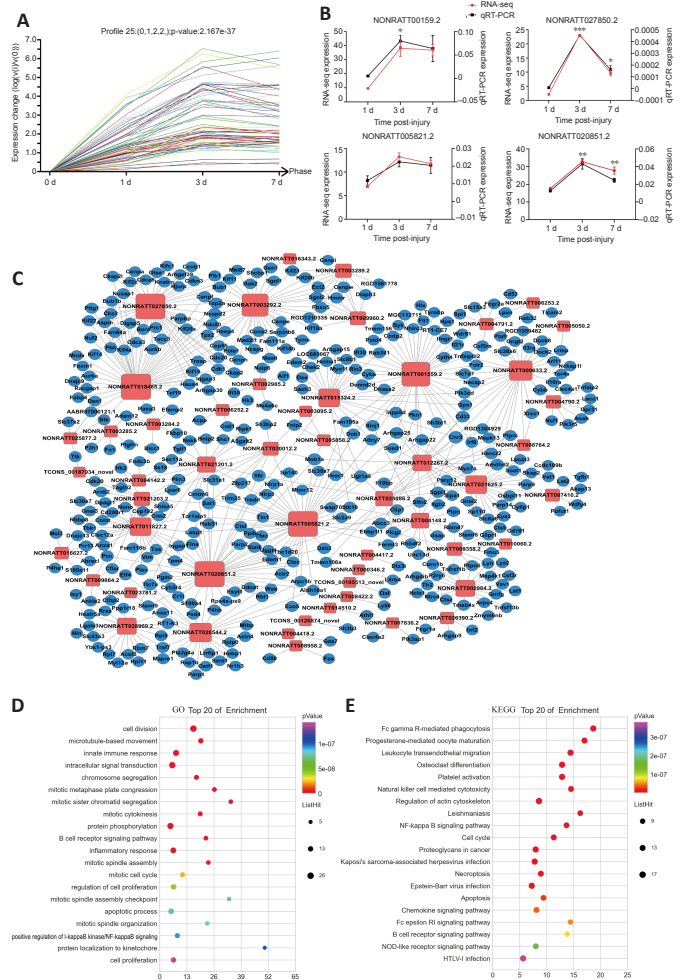

Figure 3 | RT-PCR validation and bioinformatic analysis of lncRNAs after SCI in Profile 25.
(A) RNA-sequencing trend diagram of lncRNAs in Profile 25. (B) RT-PCR validation of randomly selected lncRNAs in Profile 25. Data are expressed as mean ± SEM (*n* = 3 for each group). *P < 0.05, **P < 0.01, ***P < 0.001, *vs.* 1 day (Student's *t*-test). (C) Co-expression network for the differentially expressed lncRNA and co-expressed mRNA in Profile 25 after SCI. The blue round nodes represent mRNA, and the red square nodes indicate lncRNA. The more co-expressed genes of the lncRNA, the larger the size of the red box. Solid line between nodes indicated a positively correlated relationship between lncRNA and mRNA. (D) Bubble diagram of the top 20 enriched GO terms of co-expressed mRNAs in Profile 25. The *y*-axis shows the enriched top 20 GO terms, and the *x*-axis represents the enrichment score. The size of the bubble represents the number of co-expressed genes in the GO term. The color of the bubble represents the *P*-value of enriched GO term. (E) Bubble diagram of the top 20 enriched KEGG pathways of co-expressed mRNAs in Profile 25. The *y*-axis shows the enriched top 20 pathways, and the *x*-axis represents their enrichment score. The size of the bubble gives a measure of the number of co-expressed genes in the pathway. The color of the bubble represents the *P*-value of the enriched pathway. GO: Gene ontology; KEGG: Kyoto Encyclopedia of Genes and Genomes; LncRNA: long noncoding RNA; mRNA: messenger RNA; RT-PCR: real-time polymerase chain reaction; SCI: Spinal cord injury. The full name of mRNA can be found in the Additional Table 3.

stage includes neuronal apoptosis, axon demyelination, Waller degeneration, axon remodeling and glial scar formation (Alizadeh et al., 2019). The chronic injury stage includes cyst formation, axon necrosis and glial scar maturation (Kjell and Olson, 2016; Tran et al., 2018). In this study, we focused on the acute injury stage and the sub-acute injury stage, expecting to find key lncRNAs that participate in post-injury processes at these early stages after SCI.

The differentially co-expressed genes of lncRNAs in Profile 25 (which were up-regulated after SCI) were enriched in cell mitosis, cell proliferation, apoptosis and inflammatory response. Astrocytes and microglia play a key role during these processes. The role of astrocytes has been shown to regulate neutrophils, improve the resistance to bacterial infection and prevent bacteria from crossing the blood-brain barrier (Xie et al., 2010). Astrocytes could secrete a large number of pro-inflammatory and anti-inflammatory factors (Sofroniew, 2015). Others revealed that astrocytes can induce the differentiation and proliferation of microglia and promote the phagocytosis of microglia (Zeinstra et al., 2000). The importance of astrocytes and microglia in the early stage of SCI indicated the necessity to explore the cellular and molecular changes in astrocytes and microglia (**Figure 5**).
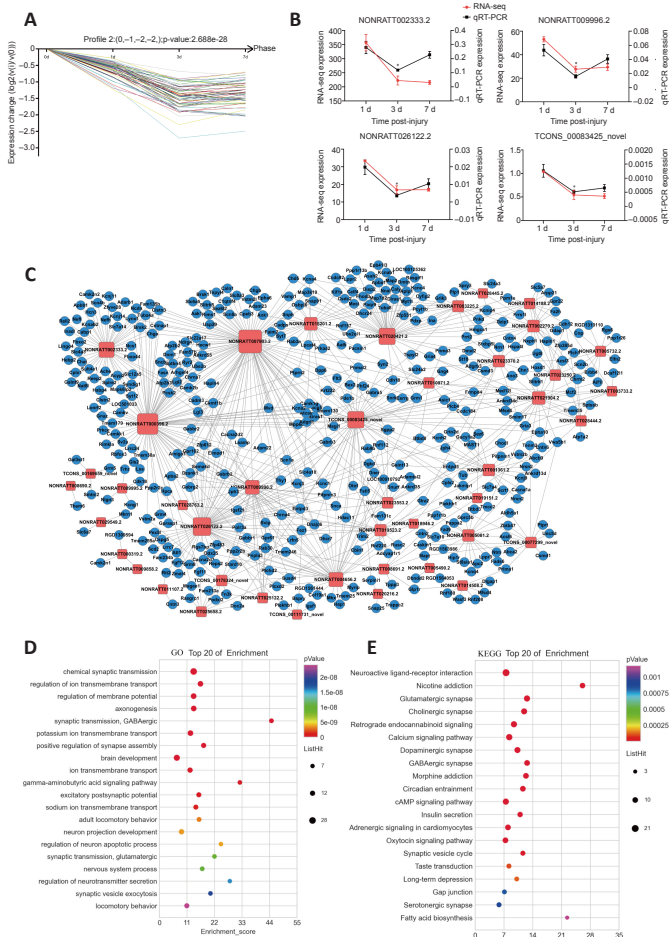
Figure 4 | RT-PCR validation and bioinformatic analysis of lncRNAs in Profile 2.
(A) RNA-sequencing trend diagram of lncRNAs in Profile 2. (B) RT-PCR validation of randomly selected lncRNAs in Profile 2. Data are expressed as mean ± SEM (n = 3 for each group). *P < 0.05, *vs.* 1 day (Student's t-test). (C) The co-expression network for the differentially expressed lncRNA and co-expressed mRNA in Profile 2 after SCI. The blue round nodes represent mRNA, and the red square nodes indicate lncRNA. The more co-expressed genes of the lncRNA, the larger the size of the red box. The solid line between nodes indicated the positively correlated relationship between lncRNA and mRNA. (D) Bubble diagram of the top 20 enriched GO terms of co-expressed mRNAs in Profile 2. The y-axis shows the enriched top 20 GO terms, and the x-axis represents their enrichment score. The size of the bubble represents the number of co-expressed genes in the GO term. The color of the bubble represents the P-value of enriched GO term. (E) Bubble diagram of the top 20 enriched KEGG pathways of co-expressed mRNAs in Profile 2. The y-axis shows the enriched top 20 pathways, and the x-axis represents their enrichment score. The size of the bubble represents the number of co-expressed genes in the pathway. The color of the bubble represents the P-value of enriched pathway. GO: Gene ontology; KEGG: Kyoto Encyclopedia of Genes and Genomes; LncRNA: long noncoding RNA; mRNA: messenger RNA; RT-PCR: real-time polymerase chain reaction; SCI: Spinal cord injury. The full name of mRNA can be found in the Additional Table 3.

The differentially co-expressed genes of lncRNAs in Profile 2 (which were down-regulated after SCI) were enriched in synaptic transmission, ion transmembrane transport, neuronal excitation, and movement. In the central nervous system, the information transmission between neurons mainly depends on synaptic transmission (Jackman and Regehr, 2017). Studies have shown that astrocytes, microglia and oligodendrocytes participate in synaptic plasticity regulation (Bar and Barak, 2019; Durkee and Araque, 2019). The major roles of astrocytes in synapses are neurotransmitter clearance, neurotransmitter release and regulation of ion balance (Goubard et al., 2011; Perez-Alvarez et al., 2014; Murphy-Royal et al., 2017). Microglia also play a very important role in synapses by regulating the release of cytokines and neurotrophic factors and in synaptic pruning (Vezzani and Viviani, 2015; Hammond et al., 2018). The oligodendrocytes form new myelin or change myelin characteristics in synapses (Sancho et al., 2021). They receive glutamatergic synapses from neurons to detect neuronal activity (Bergles et al., 2000). The pre-myelinating oligodendrocytes can activate Nav1.2 (voltage-gated channel alpha subunit 2)-driven depolarizations, in order to respond to the glutamatergic input from neighboring neurons (Berret et al., 2017). In addition, the balance between axon regeneration and synaptic function is also important for the reconstruction of functional neuronal circuits after nerve injury (Kiyoshi and Tedeschi, 2020) (**Figure 5**).

Common spinal cord injury models include contusion, full transection and hemisection injury. Contusions can better simulate clinical spinal cord
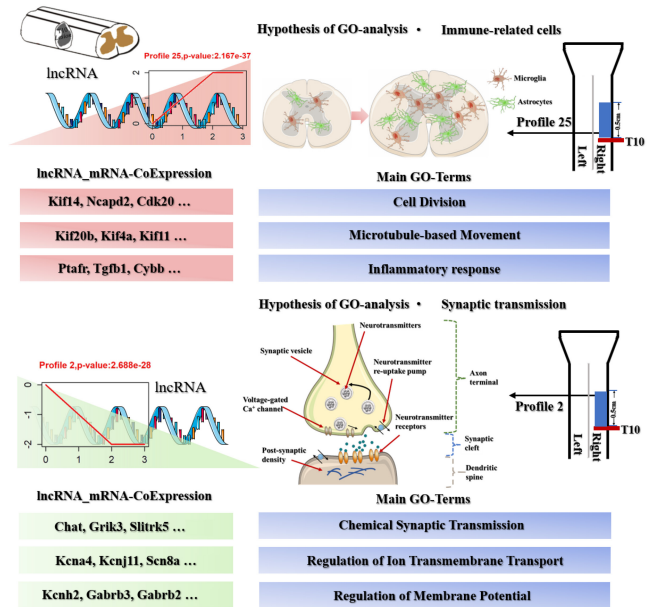

Figure 5 | Schematic diagram of changed lncRNAs, enriched biological processes, and key mRNAs in Profiles 25 and 2 after spinal cord injury.
Cdk20: Cyclin-dependent kinase 20; Chat: choline O-acetyltransferase; Cybb: cytochrome b-245, beta polypeptide; Gabrb2: gamma-aminobutyric acid A receptor, beta 2; Gabrb3: gamma-aminobutyric acid A receptor, beta 3; GO: Gene ontology; Grik3: glutamate receptor, ionotropic, kainate 3; Kcna4: potassium channel, voltage gated shaker related subfamily A, member 4; Kcnh2: potassium channel, voltage gated Eag related subfamily H, member 2; Kcnj11: potassium channel, inwardly rectifying subfamily J, member 11; Kif11: kinesin family member 11; Kif14: kinesin family member 14; Kif20b: kinesin family member 20B; Kif4a: kinesin family member 4A; LncRNA: long noncoding RNA; mRNA: messenger RNA; Ncapd2: non-SMC condensin I complex, subunit D2; Ptafr: platelet-activating factor receptor; SCI: spinal cord injury; Scn8a: sodium channel, voltage gated, type VIII, alpha subunit; Slitrk5: SLIT and NTRK-like family, member 5; Tgfb1: transforming growth factor beta 1.

injuries from car accidents, but as with all mechanical models, it is difficult to precisely control the biomechanics to produce consistent and repeatable spinal cord injuries. The full transection injury model ensures that natural or post-intervention recovery is due to repair after SCI (Jones et al., 2012), but this model is not ideal for exploring the complex pathophysiology involved in spinal cord injury because transection is not common in clinical settings. The hemisection injury model simulates an injury that is more readily seen clinically and provides a comparison between damaged and healthy fibers in the same animal. For example, hemicotomies can be used to examine motor function and recovery of different spinal tracts, or to compare functional changes in contralateral and ipsilateral lesions (Alilain et al., 2011). Therefore, in this study, we selected the semi-transverse damage model with good repeatability and stability. In the future, we will also use a variety of models to further explore the dysregulated lncRNAs after SCI.

In conclusion, we have identified a set of dysregulated lncRNAs during the early period after SCI and obtained the enriched biological processes and signaling pathways of the co-expressed genes. Our research has provided a potential research direction for SCI treatment. However, because the RNA-seq samples were obtained from mixed tissues, it was hard to determine which differentially expressed genes were associated with what cell type. And the research of the mechanism is not deep enough because we only conducted simple expression verification without any functional experiments. In future, we should perform single-cell RNA-seq to further address this issue and conduct in-depth mechanism research. The next focus would be on the chronic phase after SCI to obtain a more comprehensive view of the dysregulated lncRNAs after SCI and to identify some cells with significant changes in lncRNAs.

identical terms.

Additional files:

Additional Table 1: *The primer sequences of long noncoding RNAs for quantitative real-time polymerase chain reaction validation.*

Additional Table 2: *The differentially expressed long noncoding RNAs at different time points (0, 1, 3, 7 days) after spinal cord injury.*

Additional Table 3: *The differentially expressed mRNAs at different time points (0, 1, 3, 7 days) after spinal cord injury.*

Additional Table 4: *The data of co-expression network between long noncoding RNAs and co-expressed genes in Profile 25.*

Additional Table 5: *The enriched top 20 GO terms of co-expressed genes in Profile 25.*

Additional Table 6: *The enriched top 20 KEGG pathways of co-expressed genes in Profile 25.*

Additional Table 7: *The data of co-expression network between long noncoding RNAs and co-expressed genes in Profile 2.*

Additional Table 8: *The enriched top 20 GO terms of co-expressed genes in Profile 2.*

Additional Table 9: *The enriched top 20 KEGG pathways of co-expressed genes in Profile 2.*

References

Alilain WJ, Horn KP, Hu H, Dick TE, Silver J (2011) Functional regeneration of respiratory pathways after spinal cord injury. Nature 475:196-200.

Alizadeh A, Dyck SM, Karimi-Abdolrezaee S (2019) Traumatic spinal cord injury: an overview of pathophysiology, models and acute injury mechanisms. Front Neurol 10:282.

Anders S, Huber W (2010) Differential expression analysis for sequence count data. Genome Biol 11:R106.

Anjum A, Yazid MD, Fauzi Daud M, Idris J, Ng AMH, Selvi Naicker A, Ismail OHR, Athi Kumar RK, Lokanathan Y (2020) Spinal cord injury: pathophysiology, multimolecular interactions, and underlying recovery mechanisms. Int J Mol Sci 21:7533.

Bai YR, Lai BQ, Han WT, Sun JH, Li G, Ding Y, Zeng X, Ma YH, Zeng YS (2021) Decellularized optic nerve functional scaffold transplant facilitates directional axon regeneration and remyelination in the injured white matter of the rat spinal cord. Neural Regen Res 16:2276-2283.

Bar E, Barak B (2019) Microglia roles in synaptic plasticity and myelination in homeostatic conditions and neurodevelopmental disorders. Glia 67:2125-2141.

Bergles DE, Roberts JD, Somogyi P, Jahr CE (2000) Glutamatergic synapses on oligodendrocyte precursor cells in the hippocampus. Nature 405:187-191.

Berret E, Barron T, Xu J, Debner E, Kim EJ, Kim JH (2017) Oligodendroglial excitability mediated by glutamatergic inputs and Nav1.2 activation. Nat Commun 8:557.

Christensen MD, Everhart AW, Pickelman JT, Hulsebosch CE (1996) Mechanical and thermal allodynia in chronic central pain following spinal cord injury. Pain 68:97-107.

Durkee CA, Araque A (2019) Diversity and specificity of astrocyte-neuron communication. Neuroscience 396:73-78.

Fitch MT, Silver J (2008) CNS injury, glial scars, and inflammation: Inhibitory extracellular matrices and regeneration failure. Exp Neurol 209:294-301.

Goubard V, Fino E, Venance L (2011) Contribution of astrocytic glutamate and GABA uptake to corticostriatal information processing. J Physiol 589:2301-2319.

Hammond TR, Robinton D, Stevens B (2018) Microglia and the brain: complementary partners in development and disease. Annu Rev Cell Dev Biol 34:523-544.

Jackman SL, Regehr WG (2017) The mechanisms and functions of synaptic facilitation. Neuron 94:447-464.

Jarroux J, Morillon A, Pinskaya M (2017) History, discovery, and classification of lncRNAs. Adv Exp Med Biol 1008:1-46.

Jones CF, Lee JH, Kwon BK, Cripton PA (2012) Development of a large-animal model to measure dynamic cerebrospinal fluid pressure during spinal cord injury: laboratory investigation. J Neurosurg Spine 16:624-635.

Kiyoshi C, Tedeschi A (2020) Axon growth and synaptic function: A balancing act for axonal regeneration and neuronal circuit formation in CNS trauma and disease. Dev Neurobiol 80:277-301.

Kjell J, Olson L (2016) Rat models of spinal cord injury: from pathology to potential therapies. Dis Model Mech 9:1125-1137.

Kozuka Y, Kawamata M, Furue H, Ishida T, Tanaka S, Namiki A, Yamakage M (2016) Changes in synaptic transmission of substantia gelatinosa neurons after spinal cord hemisection revealed by analysis using in vivo patch-clamp recording. Mol Pain 12:1744806916665827.

Kwon MJ, Yoon HJ, Kim BG (2016) Regeneration-associated macrophages: a novel approach to boost intrinsic regenerative capacity for axon regeneration. Neural Regen Res 11:1368-1371.

Lin H (2019) Transplantation of adult spinal cord tissue: Transection spinal cord repair and potential clinical translation. Sci China Life Sci 62:870-872.

Mi H, Huang X, Muruganujan A, Tang H, Mills C, Kang D, Thomas PD (2017) PANTHER version 11: expanded annotation data from Gene Ontology and Reactome pathways, and data analysis tool enhancements. Nucleic Acids Res 45:D183-D189.

Mortazavi MM, Verma K, Harmon OA, Griessenauer CJ, Adeeb N, Theodore N, Tubbs RS (2015) The microanatomy of spinal cord injury: a review. Clin Anat 28:27-36.

Murphy-Royal C, Dupuis J, Groc L, Oliet SHR (2017) Astroglial glutamate transporters in the brain: Regulating neurotransmitter homeostasis and synaptic transmission. J Neurosci Res 95:2140-2151.

Ohtake Y, Park D, Abdul-Muneer PM, Li H, Xu B, Sharma K, Smith GM, Selzer ME, Li S (2014) The effect of systemic PTEN antagonist peptides on axon growth and functional recovery after spinal cord injury. Biomaterials 35:4610-4626.

Orr MB, Gensel JC (2018) Spinal cord injury scarring and inflammation: therapies targeting glial and inflammatory responses. Neurotherapeutics 15:541-553.

Percie du Sert N, Hurst V, Ahluwalia A, Alam S, Avey MT, Baker M, Browne WJ, Clark A, Cuthill IC, Dirnagl U, Emerson M, Garner P, Holgate ST, Howells DW, Karp NA, Lazic SE, Lidster K, MacCallum CJ, Macleod M, Pearl EJ, et al. (2020) The ARRIVE guidelines 2.0: Updated guidelines for reporting animal research. PLoS Biol 18:e3000410.

Perez-Alvarez A, Navarrete M, Covelo A, Martin ED, Araque A (2014) Structural and functional plasticity of astrocyte processes and dendritic spine interactions. J Neurosci 34:12738-12744.

Phang I, Werndle MC, Saadoun S, Varsos G, Czosnyka M, Zoumprouli A, Papadopoulos MC (2015) Expansion duroplasty improves intraspinal pressure, spinal cord perfusion pressure, and vascular pressure reactivity index in patients with traumatic spinal cord injury: injured spinal cord pressure evaluation study. J Neurotrauma 32:865-874.

Sancho L, Contreras M, Allen NJ (2021) Glia as sculptors of synaptic plasticity. Neurosci Res 167:17-29.

Sofroniew MV (2015) Astrocyte barriers to neurotoxic inflammation. Nat Rev Neurosci 16:249-263.

Tedeschi A, Bradke F (2017) Spatial and temporal arrangement of neuronal intrinsic and extrinsic mechanisms controlling axon regeneration. Curr Opin Neurobiol 42:118-127.

The Gene Ontology Consortium (2019) The Gene Ontology Resource: 20 years and still GOing strong. Nucleic Acids Res 47:D330-d338.

Tran AP, Warren PM, Silver J (2018) The biology of regeneration failure and success after spinal cord injury. Physiol Rev 98:881-917.

Vezzani A, Viviani B (2015) Neuromodulatory properties of inflammatory cytokines and their impact on neuronal excitability. Neuropharmacology 96:70-82.

Wilusz JE, Sunwoo H, Spector DL (2009) Long noncoding RNAs: functional surprises from the RNA world. Genes Dev 23:1494-1504.

Wu R, Mao S, Wang Y, Zhou S, Liu Y, Liu M, Gu X, Yu B (2019) Differential circular RNA expression profiles following spinal cord injury in rats: a temporal and experimental analysis. Front Neurosci 13:1303.

Xie L, Poteet EC, Li W, Scott AE, Liu R, Wen Y, Ghorpade A, Simpkins JW, Yang SH (2010) Modulation of polymorphonuclear neutrophil functions by astrocytes. J Neuroinflammation 7:53.

Yang Y, Pang M, Chen YY, Zhang LM, Liu H, Tan J, Liu B, Rong LM (2020) Human umbilical cord mesenchymal stem cells to treat spinal cord injury in the early chronic phase: study protocol for a prospective, multicenter, randomized, placebo-controlled, single-blinded clinical trial. Neural Regen Res 15:1532-1538.

Zeinstra E, Wilczak N, Streefland C, De Keyser J (2000) Astrocytes in chronic active multiple sclerosis plaques express MHC class II molecules. Neuroreport 11:89-91.

Zhang X, Wang W, Zhu W, Dong J, Cheng Y, Yin Z, Shen F (2019) Mechanisms and functions of long non-coding RNAs at multiple regulatory levels. Int J Mol Sci 20:5573.

Zhu S, Yang BS, Li SJ, Tong G, Tan JY, Wu GF, Li L, Chen GL, Chen Q, Lin LJ (2021) Protein post-translational modifications after spinal cord injury. Neural Regen Res 16:1935-1943.

Additional Table 1 The primer sequences of long noncoding RNAs for quantitative real-time polymerase chain reaction validation

Accession No.	Primer sequences (5'-3')	Amplicon size (bp)
NONRATT001559.2	Sense: CAC AGC AGA ATG GAC AAC CTT	159
	Antisense: ACA CAG TGG CAC CTA TCA TCA	
NONRATT027850.2	Sense: GGC TCA AGT GGC TAA GAA TAC C	159
	Antisense: TCC TTC ATG GAG ACA TCC TCA G	
NONRATT005821.2	Sense: TCA GTT GAG CCA ATT CCA GAT G	199
	Antisense: ACA GGA GGA GGT GAG GAG AT	
NONRATT020851.2	Sense: TTG GCA ATG GCA GTG TAT GTC	70
	Antisense: TCA AGA GCA ACG GAA CAA GAA C	
NONRATT002333.2	Sense: ATC CGT CCA GCG ATC TCA C	136
	Antisense: CGT TAC ACA GCG ACC ATC C	
NONRATT009996.2	Sense: CCA TAA CCA CTG CGA CAT TGT	151
	Antisense: GCA CCT ATG AGC CAC AGA AC	
NONRATT026122.2	Sense: GTT GCT GTG CCA CCA TAG G	136
	Antisense: CCT GCT GTC TGT TGC TGT C	
TCONS_00083425_novel	Sense: GCC GAC CTC CAC TCA TCT T	171
	Antisense: CGC TTC CTC CAG ACA CCT T	

Additional Table 5 The enriched top 20 GO terms of co-expressed genes in Profile 25

GO_id	GO_name	GO_diffgene_count	GO_gene_count	Enrichment	*P*-value	FDR	Gene name list
GO:0051301	Cell division	26	178	16.17601035	4.06E-23	8.44E-20	Kif14, Ncapd2, Cdk20, Cks2, Dsn1, Cdca8, Cenpw, Kif18b, Ccnb1, Gnai3, Cdk1, Pttg1, Cdc20, Gnai2, Mapre1, Kif2c, Aurka, Rbbp8, Kifc1, Cdca3, Knstrn, Nuf2, Reep4, Bora, Nek6, Ankle2
GO:0007018	Microtubule-based movement	13	73	19.72143728	4.58E-13	4.76E-10	Kif20b, Kif4a, Kif11, Kif2c, Kif22, Kifc1, Kif18b, Kif14, Kif20a, Kif23, Kif15, Cenpe, Kif18a, Lgals3
GO:0045087	Innate immune response	20	282	7.85414578	7.68E-12	5.32E-09	Lgals3, Nlrp3, Nlrp1a, Havcr2, Pik3cd, Btk, Trim25, Sp110, Elf4, Nlrc4, Tbk1, Anxa1, Cr1l, Tlr2, Nono, Lyn, Syk, Cybb, Cyba, Tnfaip8l2
GO:0035556	Intracellular signal transduction	24	440	6.040552118	1.31E-11	6.80E-09	Plcg2, Nlrp3, Pkn1, Vav1, Syk, Inpp5d, Sh2b3, Rasa3, Mapk13, Lyn, Gnai2, Adcy7, Shc1, Ptpn6, Mastl, Dok1, Map4k1, Akap13, Ss18, Tyrobp, Racgap1, Lat2, Ect2, Nlrp1a
GO:0007059	Chromosome segregation	11	69	17.65475377	1.29E-10	5.35E-08	Cenpf, Nek6, Knstrn, Hjurp, Top2a, Kif11, Cenpe, Pttg1, Ndc80, Cenpw, Bub1
GO:0007080	Mitotic metaphase plate congression	9	38	26.22871314	1.88E-10	6.52E-08	Cep55, Cdca8, Ccnb1, Kif2c, Cenpe, Kif18a, Kifc1, Kif14, Kif22
GO:0000070	Mitotic sister chromatid segregation	8	26	34.07490938	2.23E-10	6.62E-08	Mad2l1, Knstrn, Plk1, Dsn1, Nusap1, Kif18a, Kif18b, Cdca8, Ect2
GO:0000281	Mitotic cytokinesis	10	57	19.4286764	3.80E-10	9.87E-08	Ect2, Kif4a, Cep55, Plk1, Nusap1, Racgap1, Cenpa, Ckap2, Kif20a, Kif23
GO:0006468	Protein phosphorylation	23	496	5.135281202	9.32E-10	2.01E-07	Fnip2, Tbk1, Chek2, Aurkb, Mapk13, Bub1, Pbk, Map4k1, Stk10, Lyn, Ccnb1, Pik3cd, Cdk1, Pkn1, Tgfb1, Cdk20, Btk, Nek6, Aurka, Syk, Bub1b, Plk1, Akap13
GO:0050853	B cell receptor signaling pathway	9	45	22.1486911	9.67E-10	2.01E-07	Lat2, Lyn, Ptprc, Plcg2, Syk, Ptpn6, Btk, Nckap1l, Mnda
GO:0006954	Inflammatory response	18	305	6.535679341	1.99E-09	3.75E-07	Ptafr, Tgfb1, Cybb, Nlrp1a, Havcr2, Aif1, Nlrc4, Tlr2, Cnr2, Anxa1, Pik3cd, Fas, Nlrp3, Naip6, Cyba, Syk, Tnfrsf1b, Ncf1
GO:0090307	Mitotic spindle assembly	8	38	23.31441168	6.34E-09	1.10E-06	Kifc1, Naip6, Cdc20, Tpx2, Chek2, Nlrc4, Flna, Kif11
GO:0000278	Mitotic cell cycle	11	111	10.97457667	2.38E-08	3.81E-06	Pbk, Nuf2, Aurka, Cenpf, Cdk1, Cenpe, Cenpw, Plk1, Kif18b, Ccnb1, Mastl

GO:0042127	Regulation of cell proliferation	15	249	6.6712925	4.25E-08	6.31E-06	*Plau, Lyn, Anxa1, Cnn2, Shc1, Tnfrsf1b, Fas, Foxm1, Pla2g4a, Tgfb1, Syk, S100a11, Sat1, Stat6, Btk*
GO:0007094	Mitotic spindle assembly checkpoint	6	20	33.22303665	7.26E-08	9.89E-06	*Ttk, Mad2l1, Bub1b, Cenpe, Bub1, Plk1*
GO:0006915	Apoptotic process	17	342	5.504791648	7.78E-08	9.89E-06	*Fas, Dab2, Nlrc4, Inpp5d, Traf7, Ncf1, Gpx1, Bnip2, Cflar, Nek6, Ctsc, Cdk1, Parp1, Chek2, Tradd, Ripk1, Sp110,*
GO:0007052	Mitotic spindle organization	7	34	22.80012319	8.08E-08	9.89E-06	*Ndc80, Aurka, Aurkb, Ccnb1, Cenpe, Kif4a, Nuf2*
GO:0043123	Positive regulation of I-kappaB kinase/NF-kappaB signaling	12	157	8.464467936	9.31E-08	1.08E-05	*Tbk1, Ticam2, Ripk1, Shisa5, Ect2, Nek6, Flna, Akap13, S100a4, Cflar, Trim25, Tradd*
GO:0034501	Protein localization to kinetochore	5	11	50.33793432	1.03E-07	1.13E-05	*Mtbp, Ttk, Aurkb, Bub1b, Cdk1*
GO:0008283	Cell proliferation	14	234	6.625676825	1.43E-07	1.49E-05	*Cks2, Rap1b, Gpx1, Ncf1, Aurkb, Pola1, Map4k1, Mki67, Cdk1, Ptpn6, Tgfb1, Gnai2, Tacc3, Bub1*

GO: Gene ontology.

Additional Table 6 The enriched top 20 KEGG pathways of co-expressed genes in Profile 25

Path_id	Path_name	Path_diffgene_count	Path_gene_count	Enrichment	*P*-value	FDR	Gene name list
04666	Fc gamma R-mediated phagocytosis	15	89	18.66462733	1.37E-14	3.21E-12	*Arpc1b, Inpp5d, Lyn, Ncf1, Fcgr2a, Fcgr1a, Arpc4, Was, Dock2, Pik3cd, Ptprc, Syk, Vav1, Plcg2, Pla2g4a*
04914	Progesterone-mediated oocyte maturation	14	91	17.03745469	4.30E-13	5.04E-11	*Aurka, Kif22, Bub1, Ccna2, Plk1, Gnai3, Stk10, Ccnb1, Adcy7, Mapk13, Cdk1, Gnai2, Mad2l1, Pik3cd*
04670	Leukocyte transendothelial migration	15	115	14.44479854	6.96E-13	5.43E-11	*Sipa1, Vav1, Cyba, Pxn, Mapk13, Actn4, Cybb, Itgb2, Gnai2, Ncf1, Rap1b, Gnai3, Plcg2, Myl12a, Pik3cd*
04380	Osteoclast differentiation	15	129	12.87714599	3.87E-12	1.81E-10	*Ifngr1, Tyrobp, Spi1, Cyba, Ncf1, Lilrb4, Tgfb1, Fcgr2a, Ifnar1, Plcg2, Fcgr1a, Mapk13, Syk, Pik3cd, Btk*
04611	Platelet activation	15	129	12.87714599	3.87E-12	1.81E-10	*Pik3r5, Plcg2, Adcy7, Rap1b, Gnai2, Fermt3, Mapk13, Lyn, Btk, Gnai3, Tln1, Pik3cd, Myl12a, Syk, Pla2g4a*
04650	Natural killer cell mediated cytotoxicity	13	99	14.54206991	2.66E-11	1.04E-09	*Vav1, Fcgr2a, Ptpn6, Fas, Ifnar1, Sh3bp2, Syk, Pik3cd, Ifngr1, Shc1, Plcg2, Itgb2, Tyrobp*
04810	Regulation of actin cytoskeleton	17	219	8.596523943	8.61E-11	2.88E-09	*Rras, Tmsb4x, Cyfip1, Pxn, Actn4, Iqgap3, Diaph3, Arpc4, Itgb2, Arpc1b, Vav1, Pik3cd, Was, Myl12a, Fn1, Nckap1l, Iqgap1*
05140	Leishmaniasis	11	75	16.24237347	3.30E-10	9.21E-09	*Tlr2, Mapk13, Tgfb1, Itgb2, Ifngr1, Fcgr2a, Ncf1, Cybb, Fcgr1a, Cyba, Ptpn6*
04064	NF-kappa B signaling pathway	12	97	13.7002213	3.54E-10	9.21E-09	*Btk, Cflar, Tradd, Plau, Syk, Parp1, Ticam2, Plcg2, Ripk1, Tnfsf13b, Trim25, Lyn*
04110	Cell cycle	13	127	11.33594426	6.52E-10	1.52E-08	*Mad2l1, Ttk, Cdk1, Pttg1, Cdc20, Ccna2, Rbl1, Bub1b, Bub1, Chek2, Tgfb1, Ccnb1, Plk1*
05205	Proteoglycans in cancer	15	208	7.986306887	3.66E-09	7.79E-08	*Pxn, Fas, Fn1, Rras, Plau, Ptpn6, Ctsl, Pik3cd, Tgfb1, Iqgap1, Tlr2, Hcls1, Flna, Mapk13, Plcg2*
05167	Kaposi's sarcoma-associated herpesvirus infection	15	213	7.798834894	5.08E-09	9.91E-08	*Ifngr1, Lyn, Ifnar1, RT1-N3, Pik3cd, Tbk1, Tradd, Fas, Cd200r1, Syk, Plcg2, Gngt2, Mapk13, RT1-CE7, Pik3r5*
04217	Necroptosis	13	161	8.942018146	1.24E-08	2.23E-07	*Cflar, Fas, Pla2g4a, Tradd, Ifngr1, Ripk1, Parp1, Cybb, Stat6, Parp2, Ticam2, Nlrp3, Ifnar1*
05169	Epstein-Barr virus infection	15	229	7.253938133	1.37E-08	2.29E-07	*Pik3cd, Cdk1, Ripk1, Mapk13, Syk, Ccna2, Il10ra, RT1-N3, Plcg2, RT1-CE7, Spi1, Tbk1, Vim, Tradd, Lyn*
04210	Apoptosis	12	141	9.424974936	2.77E-08	4.33E-07	*Il3ra, Pik3cd, Fas, Ctsl, Ripk1, Parp2, Tradd, Ctsz, Cflar, Parp1, Ctsc, Ctsb*
04062	Chemokine signaling pathway	13	177	8.133700121	3.91E-08	5.72E-07	*Dock2, Gnai3, Gnai2, Pik3cd, Shc1, Lyn, Gngt2, Was, Rap1b, Vav1, Adcy7, Ncf1, Pxn*
04664	Fc epsilon RI signaling pathway	9	69	14.44479854	5.11E-08	7.03E-07	*Vav1, Inpp5d, Plcg2, Lyn, Pik3cd, Btk, Mapk13, Syk, Pla2g4a*
04662	B cell receptor signaling pathway	9	72	13.84293194	7.49E-08	9.74E-07	*Pik3cd, Pik3ap1, Ptpn6, Vav1, Btk, Plcg2, Inpp5d, Lyn, Syk*
04621	NOD-like receptor signaling pathway	12	166	8.005551	1.73E-07	2.13E-06	*Tbk1, Cyba, Nlrp1a, Nlrc4, Cybb, Mapk13, LOC685067, Ripk1, Ctsb, Nlrp3, Ifnar1, Naip6*
05166	HTLV-I infection	15	294	5.650176301	3.81E-07	4.45E-06	*Chek2, Adcy7, Pik3cd, RT1-CE7, Tln1, Pttg1, Rras, Pold4, Mad2l1, Itgb2, Cdc20, Spi1, Bub1b, Tgfb1, RT1-N3*

KEGG: Kyoto Encyclopedia of Genes and Genomes.

Additional Table 8 The enriched top 20 GO terms of co-expressed genes in Profile 2

GO_id	GO_name	GO_diffgene_count	GO_gene_count	Enrichment	*P*-value	FDR	Gene name list
GO:0007268	Chemical synaptic transmission	28	214	13.6669205	8.45E-23	1.31E-19	*Chat, Grik3, Slitrk5, Glra2, Grm1, Grm4, Grm5, Gabrb3, Chrna7, Cacna1a, Gabrb2, Chrna4, Snca, Gria4, Gabra5, Gabrg2, Grm8, Dlgap1, Snap91, Apba1, Apba2, Sncb, Nrxn2, Fgf12, Slc12a5, Clstn3, Clstn2, Camk2n1*
GO:0034765	Regulation of ion transmembrane transport	16	102	16.3849915	1.33E-14	1.03E-11	*Kcna4, Kcnj11, Scn8a, Kcnj3, Scn1a, Kcnj14, Hcn3, Kcnj9, Kcnh2, Kcnc4, Kcnc1, Cacna1a, Kcna2, Cacna2d3, Kcnq4, Cacna2d2*
GO:0042391	Regulation of membrane potential	17	130	13.6594112	4.15E-14	2.14E-11	*Kcnh2, Gabrb3, Gabrb2, Pex5l, Grik3, Cacna1a, Gabrg2, Chrna4, Dpp6, Gabra5, Glra2, Hcn3, Asic1, Chrna7, Kcnj11, Rims1, Scn1a*
GO:0007409	Axonogenesis	16	122	13.6989273	2.42E-13	9.37E-11	*Brsk2, Mapt, Snap91, Lingo4, Snap25, Cnp, Cntn2, Slitrk5, Sptbn4, Amigo1, Slitrk1, Brsk1, Rab3a, Map2, Atl1, Lrfn5*
GO:0051932	Synaptic transmission, GABAergic	9	21	44.7661376	6.57E-13	2.03E-10	*Gabrb2, Grm1, Grm4, Gabra5, Cacna1a, Clstn3, Gabrg2, Dnm1, Gabrb3*
GO:0071805	Potassium ion transmembrane transport	16	135	12.3797714	1.21E-12	3.13E-10	*Kcnc1, Kcna4, Kcnab1, Snap25, Kcnc4, Kcnh2, Kcna2, Kcnab2, Kcnq4*
GO:0051965	Positive regulation of synapse assembly	12	71	17.6542514	1.55E-11	3.43E-09	*Lrrc24, Adgrb3, Clstn2, Slitrk5, Cbln1, Slitrk1, Clstn3, Lingo4, Syndig1*
GO:0007420	Brain development	21	316	6.94158462	2.25E-11	4.34E-09	*Atp2b3, Snph, Ckmt1b, Amigo1, Kcnc1, Nefh, Gabra5, Cntn4, Kcnh2*
GO:0034220	Ion transmembrane transport	13	111	12.2333889	2.41E-10	4.14E-08	*Gabrg2, Chrna7, Gria4, Gria3, Gabrb3, Ryr2, Chrna4, Gabrb2, Grik3*
GO:0007214	Gamma-aminobutyric acid signaling pathway	8	26	32.1397911	3.54E-10	5.47E-08	*Gabra5, Gabrb3, Cacna1a, Gabbr2, Gabrb2, Phf24, Gabbr1, Gabrg2, Glra2*
GO:0060079	Excitatory postsynaptic potential	11	73	15.7396922	4.52E-10	6.36E-08	*Glra2, Chrna4, Gria3, Snca, Gria4, Grin2d, Grik3, Sez6, Nlgn3*
GO:0035725	Sodium ion transmembrane transport	11	79	14.5442725	1.09E-09	1.41E-07	*Scn8a, Slc4a10, Scn4b, Slc8a3, Hcn3, Slc24a2, Asic1, Scn1a, Scn2b*
GO:0008344	Adult locomotory behavior	10	66	15.8264123	3.03E-09	3.61E-07	*Fgf12, Snca, Dnm1, Scn8a, Atp1a2, Sez6l2, Adam22, Grin2d, Cnp*

GO ID	Term	Count	Total	Fold	P-value	FDR	Genes
GO:0031175	Neuron projection development	14	166	8.80940057	3.67E-09	3.97E-07	*Atcay, Cyfip2, Cntnap1, Rasgrf1, Cntn4, Hap1, Nefh, Ncdn, Cntn2*
GO:0043523	Regulation of neuron apoptotic process	8	34	24.5774873	3.85E-09	3.97E-07	*Gabra5, Faim2, Snrk, Snca, Gabrb2, Trim2, Gabrb3, Grm4, Grm8*
GO:0035249	Synaptic transmission, glutamatergic	8	38	21.9903834	1.00E-08	9.69E-07	*Grm8, Grm4, Gria4, Grik3, Grin2d, Clstn3, Cacna1a, Gria3, Chrna4*
GO:0050877	Nervous system process	9	55	17.0925253	1.07E-08	9.69E-07	*Chrna4, Gabrb2, Glra2, Gabrb3, Cacna1a, Gabrg2, Chrna7, Kcnj11, Gabra5*
GO:0046928	Regulation of neurotransmitter secretion	7	26	28.1223172	1.57E-08	1.35E-06	*Syt12, Snca, Syn2, Cplx2, Cplx1, Grm8, Kcnc4, Doc2a, Adgrl1*
GO:0016079	Synaptic vesicle exocytosis	8	41	20.3813309	1.91E-08	1.55E-06	*Doc2a, Adgrl1, Otof, Apba2, Cplx2, Rab3a, Apba1, Cplx1, Scn8a*
GO:0007626	Locomotory behavior	11	105	10.9428336	2.41E-08	1.86E-06	*Scn8a, Apba1, Pde1b, Gprc5b, Snap25, Ppp1r1b, Chrna4, Grm1, Apba2*

GO: Gene ontology.

Additional Table 9 The enriched top 20 KEGG pathways of co-expressed genes in Profile 2

Path_id	Path_name	Path_diffgene_count	Path_gene_count	Enrichment	*P*-value	FDR	Gene name list
04080	Neuroactive ligand-receptor interaction	21	292	7.51212582	4.98E-12	8.57E-10	*Grm5, Gabrb3, Glp1r, Chrna7, Gabrb2, Trhr, Chrna4, Gria3, Adcyap1r1, Glra2, Grin2d, Grm1, Grm4, Gabbr1, Gabbr2, Grik3, Grm8, Gria4, Gabra5, Gabrg2, Chrm2*
05033	Nicotine addiction	10	40	26.1135803	1.52E-11	1.31E-09	*Gabrg2, Chrna4, Gria3, Gria4, Gabra5, Grin2d, Gabrb3, Chrna7, Cacna1a, Gabrb2*
04724	Glutamatergic synapse	14	116	12.606556	2.90E-11	1.67E-09	*Grik3, Grin2d, Gng4, Gls2, Cacna1a, Gria3, Gria4, Dlgap1, Grm8, Grm1, Grm4, Kcnj3, Plcb4, Grm5*
04725	Cholinergic synapse	13	114	11.9114577	3.39E-10	1.46E-08	*Slc5a7, Camk2b, Plcb4, Kcnq4, Gng4, Kcnj14, Chat, Kcnj3, Chrna7, Cacna1a, Chrna4, Chrm2, Ache*
04723	Retrograde endocannabinoid signaling	14	155	9.43458383	1.48E-09	5.10E-08	*Grm5, Grm1, Gng4, Kcnj9, Gabrb3, Gabrg2, Kcnj3, Rims1, Plcb4, Cacna1a, Gabrb2, Gria3, Gria4, Gabra5*
04020	Calcium signaling pathway	15	189	8.29002548	2.15E-09	5.30E-08	*Atp2b2, Chrm2, Ryr2, Slc8a3, Atp2b3, Pde1b, Erbb4, Camk2b, Grin2d, Grm1, Grm5, Plcb4, Chrna7, Cacna1a, Trhr*
04728	Dopaminergic synapse	13	132	10.287168	2.16E-09	5.30E-08	*Gng4, Kcnj9, Caly, Scn1a, Ppp2r2b, Kcnj3, Plcb4, Ppp1r1b, Gria4, Ppp2r2c, Cacna1a, Gria3, Camk2b*
04727	GABAergic synapse	11	91	12.6263465	5.16E-09	1.11E-07	*Gabbr2, Gabbr1, Gng4, Gls2, Gabrg2, Gabra5, Gabrb3, Slc12a5, Hap1, Cacna1a, Gabrb2*
05032	Morphine addiction	11	93	12.3548122	6.53E-09	1.25E-07	*Gabbr1, Gng4, Kcnj9, Gabbr2, Cacna1a, Gabrb2, Kcnj3, Gabrb3, Gabrg2, Pde1b, Gabra5*
04713	Circadian entrainment	11	99	11.6060357	1.28E-08	2.21E-07	*Ryr2, Gng4, Kcnj9, Adcyap1r1, Plcb4, Gria3, Gucy1a2, Kcnj3, Grin2d, Gria4, Camk2b*
04024	cAMP signaling pathway	14	196	7.46102293	3.16E-08	4.95E-07	*Camk2b, Grin2d, Glp1r, Adcyap1r1, Gria3, Gria4, Gabbr2, Atp2b3, Atp2b2, Gabbr1, Atp1a2, Chrm2, Ppp1r1b, Ryr2*
04911	Insulin secretion	9	86	10.9312662	5.94E-07	8.51E-06	*Ryr2, Plcb4, Kcnj11, Adcyap1r1, Camk2b, Rab3a, Glp1r, Atp1a2, Snap25*
04261	Adrenergic signaling in cardiomyocytes	11	144	7.97914952	6.48E-07	8.58E-06	*Atp2b2, Ppp2r2c, Cacna2d2, Atp1a2, Scn4b, Atp2b3, Camk2b, Plcb4, Ryr2, Cacna2d3, Ppp2r2b*
04921	Oxytocin signaling pathway	11	156	7.36536879	1.46E-06	1.79E-05	*Camk1g, Kcnj9, Prkaa2, Cacna2d2, Gucy1a2, Kcnj14, Kcnj3, Ryr2, Camk2b, Cacna2d3, Plcb4*
04721	Synaptic vesicle cycle	7	63	11.6060357	9.76E-06	0.000112	*Cplx1, Cacna1a, Dnm1, Snap25, Rims1, Rab3a*
04742	Taste transduction	7	89	8.21550839	9.83E-05	0.0010562	*Gabra5, Grm1, Pde1b, Grm4, Gabbr2, Gabbr1, Cacna1a*
04730	Long-term depression	6	62	10.1084827	0.000116	0.001174	*Plcb4, Cacna1a, Gria3, Grm1, Gnaz, Gucy1a2*
04540	Gap junction	6	88	7.12188552	0.0008302	0.0079328	*Tuba8, Grm1, Tuba4a, Gucy1a2, Plcb4, Grm5*
04726	Serotonergic synapse	7	126	5.80301783	0.00089	0.0080569	*Cacna1a, Kcnj9, Gabrb3, Kcnj3, Gabrb2, Plcb4, Gng4*
00061	Fatty acid biosynthesis	3	14	22.3830688	0.0011725	0.0100831	*Fasn, Acsl3, Acsl6*

KEGG: Kyoto Encyclopedia of Genes and Genomes.